Magnetic-field-free nonreciprocal transport in graphene multiterminal Josephson junctions

Fan Zhang,[1,‡] Asmaul Smitha Rashid,[2,‡] Mostafa Tanhayi Ahari,[3] George J. de Coster,[4] Takashi Taniguchi,[5] Kenji Watanabe,[6] Matthew J. Gilbert,[7,3] Nitin Samarth,[1,8,*] and Morteza Kayyalha[2,†]

[1] *Department of Physics, The Pennsylvania State University, University Park, Pennsylvania 16802, USA*
[2] *Department of Electrical Engineering, The Pennsylvania State University, University Park, Pennsylvania 16802, USA*
[3] *Materials Research Laboratory, The Grainger College of Engineering, University of Illinois, Urbana-Champaign, Illinois 61801, USA*
[4] *DEVCOM Army Research Laboratory, 2800 Powder Mill Rd, Adelphi, Maryland 20783, USA*
[5] *International Center for Materials, Nanoarchitectonics, National Institute for Materials Science, 1-1 Namiki, Tsukuba 305-0044, Japan*
[6] *Research Center for Functional Materials, Institute for Materials Science, 1-1 Namiki, Tsukuba 305-0044, Japan*
[7] *Department of Electrical Engineering, University of Illinois, Urbana-Champaign, IL 61801, USA*
[8] *Department of Materials Science and Engineering, The Pennsylvania State University, University Park, Pennsylvania 16802, USA*

(Received 20 July 2023; revised 12 October 2023; accepted 12 February 2024; published 8 March 2024)

Nonreciprocal superconducting devices have attracted growing interest in recent years as they potentially enable directional charge transport for applications in superconducting quantum circuits. Specifically, the superconducting diode effect has been explored in two-terminal devices that exhibit superconducting transport in one current direction while showing dissipative transport in the opposite direction. Here, we exploit multiterminal Josephson junctions (MTJJs) to engineer magnetic-field-free nonreciprocity in multiport networks. We show that when treated as a two-port electrical network, a three-terminal Josephson junction (JJ) with an asymmetric graphene region exhibits reconfigurable two-port nonreciprocity. We observe nonreciprocal (reciprocal) transport between superconducting terminals with broken (preserved) spatial mirror symmetry. We explain our observations by considering a circuit network of JJs with different critical currents.

DOI: 10.1103/PhysRevApplied.21.034011

I. INTRODUCTION

In two-terminal electronic devices, the concept of reciprocity implies a symmetry relation between the applied current and measured voltage. In other words, the resistance remains the same if the polarity of the current source is reversed from positive to negative [1]. Violating this fundamental symmetry in semiconductor technology has led to the development of a wide range of established device technologies, such as diodes, transistors, rectifiers, and photodetectors [2–5]. In superconducting devices, engineering nonreciprocity requires simultaneous breaking of time-reversal and inversion symmetries [6–16]. Current experimental demonstrations of nonreciprocity in superconductors have focused on two-terminal configurations where nonreciprocity emerges as the superconducting diode effect (SDE) [17–23], [23–27]. In these two-terminal devices, the SDE has been identified by demonstrating asymmetric critical currents for the positive and negative current polarities, i.e., $I_c^+ \neq I_c^-$.

The SDE has also been reported in multiterminal Josephson junctions (MTJJs) [28,29]. These studies, however, have treated MTJJs as two-terminal devices and reported nonreciprocity either under a small magnetic field [28] or with an applied current bias [29]. Here, we construct devices based on MTJJs to demonstrate reconfigurable and magnetic-field-free nonreciprocal transport in multiport networks. We find that in MTJJs, a current I_j applied to terminal j results in a critical current $I_{c,kj}$ at terminal k. We observe two-port nonreciprocal transport (i.e., $I_{c,jk} \neq I_{c,kj}$), if the spatial mirror symmetry between terminals j and k is broken. Notably, we show that this two-port

*nsamarth@psu.edu
†mzk463@psu.edu
‡These authors contributed equally to this work.

nonreciprocity is polarity independent ($I^{\pm}_{c,jk} \neq I^{\pm}_{c,kj}$) and emerges without any magnetic field or bias current. We design devices with asymmetric channel regions that allow us to break spatial mirror symmetry between specific terminals. We further control the efficiency of nonreciprocal transport by controlling the degree of asymmetry in the channel. Furthermore, using a circuit-network model of Josephson junctions (JJs), we show that the efficiency depends on the asymmetry of the JJs and reaches a maximum value of 30%. Our model is materials agnostic and applies to a broad range of junctions with sinusoidal CPRs, regardless of the Fermi surface or the band structure of the normal material [28].

MTJJs have recently attracted increasing interest due to their potential to create superconducting properties such as quartet pairings [30–41] and to emulate higher-dimensional topological phases [42–44]. Here, we treat a MTJJ with n superconducting terminals as a $(n-1)$-port network. The reciprocity relation for multiport networks states that a network is reciprocal when a voltage V_k (at port k) produced by a current I_j (injected to port j) remains the same if the current and voltage leads are exchanged [1,45–47]. Figure 1(a) schematically demonstrates this reciprocity relation in a two-port network. Following this definition, we find that in MTJJs, a current I_j applied to terminal j results in a critical current ($I_{c,kj}$) at terminal k. We define this critical current as the maximum current I_j for which $V_k = 0$. Likewise, a current I_k applied to terminal k results in a critical current $I_{c,jk}$ at terminal j. Therefore, we consider the MTJJ nonreciprocal if $I_{c,jk} \neq I_{c,kj}$. We explore this nonreciprocity in three- and four-terminal graphene JJs. We intentionally create a graphene channel with an asymmetric geometry to break the spatial mirror symmetry between some of the terminals. In these asymmetric MTJJs, we observe reconfigurable two-port nonreciprocity: transport is nonreciprocal between terminals with broken spatial mirror symmetry, whereas it is reciprocal between terminals with preserved spatial mirror symmetry. We use a circuit network of JJs with different critical currents to explain the observed nonreciprocity in our MTJJs.

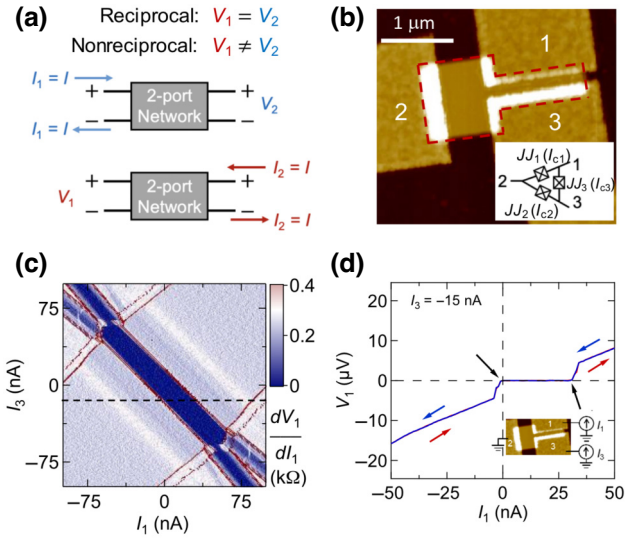

FIG. 1. (a) Schematic of a two-port network. A current I applied to port 1 ($I_1 = I$) while $I_2 = 0$ will produce a voltage V_2 at port 2. Likewise, the same current I applied to port 2 ($I_2 = I$) while $I_1 = 0$ will produce a voltage V_1 at port 1. The network is reciprocal if $V_1 = V_2$, whereas it is nonreciprocal if $V_1 \neq V_2$. (b) An AFM image of a representative three-terminal JJ. The JJ is made of *h*-BN/graphene/*h*-BN heterostructure (marked by the red dashed contour) edge contacted with Ti/Al superconducting terminals. The inset is a schematic of the circuit network of coupled JJs utilized to model the three-terminal JJ. (c) Color map of the differential resistance dV_1/dI_1 versus I_1 and I_3. (d) A horizontal cut of V_1 versus I_1 along the black dashed line ($I_3 = -15$ nA) in (c). Red and blue arrows mark I_1 sweep directions. The black arrows mark the position of the critical current for positive and negative currents. All the measurements are performed at $V_g = 30$ V, $B = 0$ T, and $T = 250$ mK.

II. DEVICE CONFIGURATION

We fabricate our MTJJs on *h*-BN/graphene/*h*-BN van der Waals heterostructures, which are edge-contacted by Ti(10 nm)/Al(100 nm) superconducting electrodes. Figure 1(b) shows an atomic-force-microscope (AFM) image of a representative three-terminal JJ. The graphene channel in this device is narrower (approximately 400 nm) between terminals (1, 3), whereas it is wider (approximately 700 nm) between terminals (1, 2) and (2, 3). The inset of Fig. 1(b) shows the circuit network of JJs representing our three-terminal device. We use three JJs (JJ1, JJ2, JJ3) between each terminal pair with corresponding critical currents (I_{c1}, I_{c2}, I_{c3}). Because the graphene region has an asymmetric geometry, the critical current of JJ3 (I_{c3}) is larger than the critical current of JJ1 (I_{c1}) and JJ2 (I_{c2}), whereas JJ1 and JJ2 have approximately similar critical currents, i.e., $I_{c3} > I_{c1} \approx I_{c2}$. We characterize our three-terminal JJs using two different bias-current configurations. In the first configuration (config. 1), we ground terminal 2 and apply currents I_1 and I_3 to terminals 1 and 3, respectively. In the second configuration (config. 2), we ground terminal 3 and apply currents I_1 and I_2 to terminals 1 and 2, respectively. We perform all the measurements at gate voltage $V_g = 30$ V, magnetic field $B = 0$ T, and temperature $T = 250$ mK, unless specified otherwise. We choose $T = 250$ mK to avoid Joule heating and stochastic switching noise [48,49] (see Appendix A for more details).

III. RECONFIGURABLE MULTIPORT NONRECIPROCITY

Figure 1(c) shows a color map of the differential resistance dV_1/dI_1 as a function of the bias currents I_1 and I_3 measured in the three-terminal JJ using config. 1. The

boundary of the dark blue region marks the critical current contour (CCC). We observe that the CCC in this configuration is asymmetric; it is titled by approximately 45° along the $V_1 - V_3 = 0$ direction. This is because the critical current of JJ3 (I_{c3}) is larger compared to the critical currents of JJ1 (I_{c1}) and JJ2 (I_{c2}); see Fig. 1(b). We also observe that at a nonzero value of I_3, the critical current along the I_1 direction becomes asymmetric for the positive and negative current polarities. Here, we define the critical current as the maximum of the total current in terminal 1 that results in $V_1 = 0$. To highlight this asymmetry, Fig. 1(d) plots a cut of V_1-I_1 along the horizontal dashed line in Fig. 1(c) at $I_3 = -15$ nA. We observe that the critical current for the positive current polarity is around 31 nA, whereas the critical current for the negative current polarity is around 0 nA. We also note that the return currents are the same as the critical currents at $T = 250$ mK, indicating there is no Joule heating at this temperature.

The asymmetry of the critical current for positive and negative polarities ($I_c^+ \neq I_c^-$) has been used to define the SDE in single-port networks (two-terminal devices) [17–23], [23–27]. In MTJJs, this asymmetry depends on the bias current I_3 and has been considered as a signature of the SDE with a diode efficiency of approximately 100% [29]. However, this single-port definition of nonreciprocity is not applicable in multiport networks [27]. This is because the additional bias current I_3 may partially cancel out the current in terminal 1 (I_1), thereby shifting the critical current of this terminal toward either a positive or negative polarity (i.e., $I_{c1}^+ \neq I_{c1}^-$). Therefore, even for a reciprocal junction, this single-port definition of nonreciprocity may give an erroneous impression that transport is nonreciprocal. The limitations of this single-port definition of nonreciprocity are better showcased in the thought experiment discussed in Appendix E. In the following, we will evaluate our MTJJs using the multiport definition of nonreciprocity.

We consider MTJJs as multiport networks and accordingly define the efficiency tensor for nonreciprocal transport as follows:

$$\eta_{jk}^{\vartheta} = \frac{|I_{c,jk}^{\vartheta}| - |I_{c,kj}^{\vartheta}|}{|I_{c,jk}^{\vartheta}| + |I_{c,kj}^{\vartheta}|}, \tag{1}$$

where $\vartheta = \pm$ specifies the input current polarity and $I_{c,jk}^{\vartheta}$ denotes the critical current tensor, which is defined as the maximum or minimum current I_k for which the voltage at terminal j remains zero:

$$I_{c,jk}^{+} = \max\left[I_k\right]_{V_j=0}, \quad I_{c,jk}^{-} = \min\left[I_k\right]_{V_j=0}, \\ I_\ell = 0, \quad \forall\, \ell \neq j. \tag{2}$$

We first focus on the three-terminal JJ in confing. 1, where terminal 2 is grounded and a two-port network is formed between terminals 1 and 3. Figure 2 plots the voltage-current characteristics of the three-terminal JJ. Following Eq. (2), we extract the critical currents $I_{c,11}^{\pm}$, $I_{c,31}^{\pm}$, $I_{c,13}^{\pm}$, and $I_{c,33}^{\pm}$, which are marked by arrows. We note that these critical currents are independent of the polarity of the applied current, i.e., $|I_{c,jk}^{+}| = |I_{c,jk}^{-}|$ where $j, k = 1, 3$. We find that $|I_{c,11}^{\pm}| = |I_{c,13}^{\pm}| = |I_{c,31}^{\pm}| = |I_{c,33}^{\pm}| = 15.75$ nA, indicating that transport is reciprocal in this configuration.

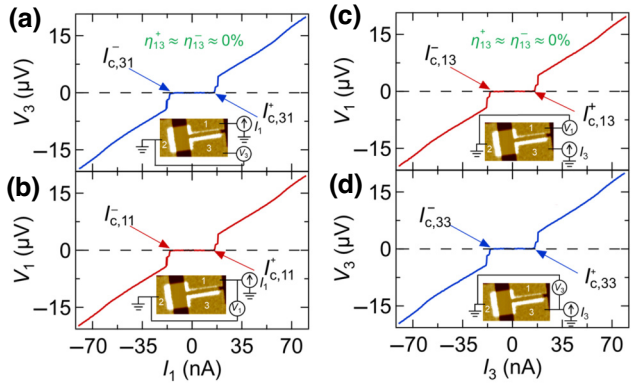

FIG. 2. Voltage-current characteristics of the three-terminal JJ in config. 1. (a),(b) Voltages V_3 (a) and V_1 (b) as a function of the bias current I_1 at $I_3 = 0$ nA. (c),(d) Voltages V_1 (c) and V_3 (d) as a function of the bias current I_3 at $I_1 = 0$ nA. The inset in each panel shows the measurement configuration. In each measurement, I_1 (or I_3) is swept from 0 to 100 nA in the positive direction and from 0 to −100 nA in the negative direction. The critical currents are labeled as $I_{c,13}^{\pm}$, $I_{c,31}^{\pm}$, $I_{c,11}^{\pm}$, and $I_{c,33}^{\pm}$.

We explain this observation by considering the circuit network of coupled JJs shown in the inset of Fig. 1(b). In Figs. 2(a) and 2(b), I_1 splits between JJ1, and JJ2 in series with JJ3. Since terminals 1 and 3 are mirror symmetric ($I_{c1} \approx I_{c2}$), JJ1 and JJ2 transition to the normal state simultaneously once $I_1 > I_{c1} + I_{c2} \approx 2I_{c1}$. As a result, a nonzero voltage develops across terminals 1 ($V_1 \neq 0$) and 3 ($V_3 \neq 0$). Following Eq. (2), we find $I_{c,11}^{+} \approx I_{c,31}^{+} \approx 2I_{c1}$. Likewise, in Figs. 2(c) and 2(d), I_3 splits between JJ2, and JJ1 in series with JJ3. Similarly in this case, JJ1 and JJ2 transition to the normal state once $I_3 > I_{c1} + I_{c2} \approx 2I_{c1}$. Following Eq. (2), we find that $I_{c,13}^{+} \approx I_{c,33}^{+} \approx 2I_{c1}$. Therefore, all the critical currents are the same in this configuration. Considering $I_{c,11}^{+} \approx 2I_{c1} \approx 15.75$ nA, we estimate $I_{c1} \approx I_{c2} \approx 7.88$ nA. We now investigate the transport properties of the three-terminal JJ in config. 2, where terminal 3 is grounded and a two-port network is formed between terminals 1 and 2 (see Appendix B for differential resistance maps in this configuration). Figure 3 plots the voltage-current characteristics of the three-terminal JJ in config. 2, where the critical currents $I_{c,11}^{\pm}$, $I_{c,21}^{\pm}$, $I_{c,12}^{\pm}$, and $I_{c,22}^{\pm}$ are marked by arrows. Similar to config. 1, the critical currents are identical for both polarities of the applied current, i.e., $|I_{c,jk}^{+}| = |I_{c,jk}^{-}|$ where $j, k = 1, 2$. Notably, we find

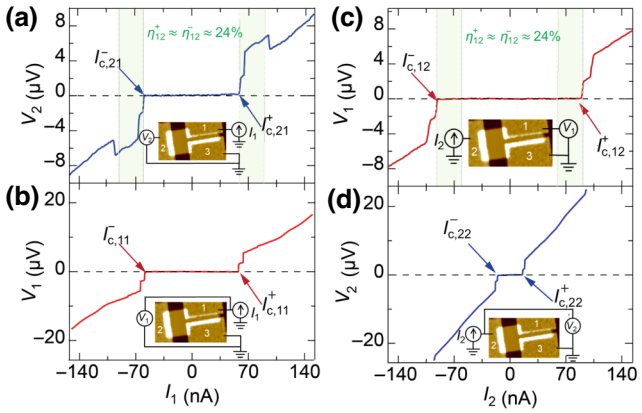

FIG. 3. Voltage-current characteristics of the three-terminal JJ in config. 2. (a),(b) Voltages V_2 (a) and V_1 (b) as a function of the bias current I_1 at $I_2 = 0$ nA. (c),(d) Voltages V_1 (c) and V_2 (d) as a function of the bias current I_2 at $I_1 = 0$ nA. The inset in each panel shows the measurement configuration. In each measurement, I_1 (or I_2) is swept from 0 to 150 nA in the positive direction and from 0 to −150 nA in the negative direction. The critical currents are labeled as $I^{\pm}_{c,12}$, $I^{\pm}_{c,21}$, $I^{\pm}_{c,11}$, and $I^{\pm}_{c,22}$. Shaded areas in (a),(c) mark the range of the current in which transport is nonreciprocal. The efficiency of two-port nonreciprocity $\eta^{\pm}_{12} = (|I^{\pm}_{c,12}| - |I^{\pm}_{c,21}|)/(|I^{\pm}_{c,12}| + |I^{\pm}_{c,21}|)$ are calculated from the critical currents as $\eta^{+}_{12} \approx \eta^{-}_{12} \approx 24\%$.

that $I^{\pm}_{c,12} \neq I^{\pm}_{c,21}$, indicating that transport is nonreciprocal within the shaded regions in Figs. 3(a) and 3(c). Table I summarizes the extracted values of the critical current for both configurations.

The observed nonreciprocity in config. 2 arises from the broken spatial mirror symmetry between terminals 1 and 2. We explain this nonreciprocity by considering the circuit network of the coupled JJs as shown in the inset of Fig. 1(b). When the current I_1 is applied to terminal 1 but terminal 2 is floating [Figs. 3(a) and 3(b)], I_1 splits between JJ3, and JJ1 in series with JJ2. Once $I_1 > I_{c3} + I_{c1}$, all three JJs simultaneously transition to the normal state, resulting in nonzero V_1 and V_2. From Eq. (2), we estimate $I^{+}_{c,11} \approx I^{+}_{c,21} \approx I_{c3} + I_{c1}$. We also experimentally extract $I^{+}_{c,11} \approx I^{+}_{c,21} \approx 57.25$ nA (Table I). Therefore, $I_{c3} + I_{c1} \approx 57.25$ nA. Considering the value of $I_{c1} \approx I_{c2} = 7.88$ nA obtained in config. 1, we estimate $I_{c3} \approx 49.4$ nA.

TABLE I. The critical-current tensor measured in both configurations.

Config. 1	$\lvert I^{\pm}_{c,11}\rvert$	15.75 nA
	$\lvert I^{\pm}_{c,13}\rvert$	15.75 nA
	$\lvert I^{\pm}_{c,31}\rvert$	15.75 nA
	$\lvert I^{\pm}_{c,33}\rvert$	15.75 nA
Config. 2	$\lvert I^{\pm}_{c,11}\rvert$	57.5 nA
	$\lvert I^{\pm}_{c,12}\rvert$	94.25 nA
	$\lvert I^{\pm}_{c,21}\rvert$	57.25 nA
	$\lvert I^{\pm}_{c,22}\rvert$	15.75 nA

On the other hand, when the current I_2 is applied to terminal 2 but terminal 1 is floating [Figs. 3(c) and 3(d)], I_2 splits between JJ2, and JJ1 in series with JJ3. In this case, when $I_2 > I_{c1} + I_{c2} \approx 2I_{c1}$, JJ1 and JJ2 simultaneously transition to the normal state, resulting in nonzero V_2. Following Eq. (2), we estimate $I^{+}_{c,22} \approx 2I_{c1} \approx 15.75$ nA, which is consistent with $I^{+}_{c,22} \approx 15.75$ nA that we obtain experimentally (Table I). However, because $I_{c3} \approx 49.4$ nA $> I_{c1} + I_{c2} \approx 15.75$ nA, JJ3 remains in the superconducting state, resulting in $V_1 = 0$. The current flow in JJ3 depends on the ratio of the normal-state resistances between JJ1 (R_1) and JJ2 (R_2), i.e., $I_{JJ3} \approx (R_2/(R_2 + R_1))I_2$. Assuming $R_1 \approx R_2$, $I_2 \approx 2I_{JJ3}$. Therefore, when $I_{JJ3} > I_{c3}$ or $I_2 > 2I_{c3}$, JJ3 transitions to the normal state, resulting in a nonzero V_1. From this analysis, we estimate $I^{+}_{c,12} = 2I_{c3} \approx 98.8$ nA, which is consistent with $I^{+}_{c,12} = 94.25$ nA that we obtain experimentally (Table I). We further calculate the nonreciprocal efficiency of this two-port network [Eq. (1)] as $\eta^{+}_{12} \approx \eta^{-}_{12} \approx 24\%$ (see Appendix G for results from a more symmetric device). We finally note that, based on our above analysis, this efficiency is maximized when $I_{c3} \gg I_{c1} \approx I_{c2}$. In this case, $I_{c,12} = 2I_{c3}$ and $I_{c,21} = I_{c3} + I_{c1} \approx I_{c3}$, resulting in $\eta^{\pm}_{12} \approx 33\%$.

To better understand the limits of the efficiency, we have performed numerical simulations of our circuit-network model using resistively shunted junctions (RSJs). In our simulations, we consider the ratio between the critical currents of JJ3 and JJ1/JJ2 as a representation of the spatial mirror symmetry breaking (i.e., $x = I_{c3}/I_{c1} = I_{c3}/I_{c2}$). In this case, $x = 1$ represents the perfect mirror symmetry and results in zero efficiency. Our modeling shows that the efficiency increases monotonically with increasing x and eventually reaches a theoretical limit of 30% (see Appendix G for more details). Finally, we note that because there are both dissipative (JJ1 and JJ2) and superconducting (JJ3) channels during the measurement of $I^{\pm}_{c,12}$, the observed nonreciprocity in our three-terminal JJ is different from the purely superconducting SDE observed in two-terminal JJs. Our combined results from configs. 1 and 2 indicate that two-port nonreciprocity can be engineered in MTJJs by changing the device geometry and/or measurement configurations.

To investigate the role of a control bias current on the two-port nonreciprocity, we study an asymmetric four-terminal JJ. Figure 4(a) plots $I^{\pm}_{c,24}$ and $I^{\pm}_{c,42}$ as a function of I_1. Inset of Fig. 4(a) shows the AFM image of the device as well as the measurement configuration. We ground terminal 3 and apply currents I_2 and I_4 while keeping I_1 constant. In this case, we can treat the four-terminal JJ as a three-port network (between terminals 1, 2, and 4). Following Eq. (2), we extract the critical-current tensor at zero and nonzero values of I_1. Figure 4(b) plots the efficiency of

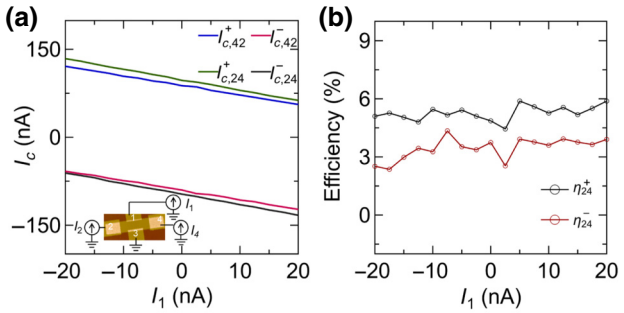

FIG. 4. (a) Critical currents versus the bias current I_1 extracted from *V-I* characteristics of a four-terminal JJ. Inset shows the measurement configuration. Here, terminal 3 is grounded and I_1 is kept at a constant value during each measurement. (b) Efficiency of nonreciprocal transport $\eta_{24}^{\pm}$ as a function of I_1.

nonreciprocal transport as a function of I_1. Because terminals 2 and 4 are mirror symmetric, we would expect no nonreciprocal transport. However, $\eta_{24}^{+} \approx \eta_{24}^{-} \approx 4\%$. We speculate that because of the imperfect fabrication process, the contact transparency is slightly different between terminals 2 and 4, resulting in nonzero but negligible $\eta_{24}^{\pm}$.

From Fig. 4(a), we observe that $I_{c,24}^{\pm}$ and $I_{c,42}^{\pm}$ change almost linearly with I_1. However, the difference between $I_{c,24}^{\pm}$ and $I_{c,42}^{\pm}$ does not change significantly with I_1. Therefore, η_{24}^{+} and η_{24}^{-} remain independent of I_1. We note that the geometry of the four-terminal JJ [inset of Fig. 4(a)] is such that terminals 2 and 4 are mirror symmetric even for $I_1 \neq 0$. Therefore, our observations indicate that the effect of the control current (I_1) on two-port nonreciprocity is negligible compared to the spatial mirror symmetry of the terminals (see Appendix D for additional measurements between terminals 1 and 2).

IV. CONCLUSION

In conclusion, we have studied multiport nonreciprocal transport in MTJJs. Following the reciprocal relation in two-port electrical networks, we have developed a definition of two-port nonreciprocity for MTJJs. We have also explored transport properties of three- and four-terminal JJs with asymmetric graphene channels. We have shown that the MTJJ exhibits magnetic-field-free nonreciprocal (reciprocal) transport if spatial mirror symmetry is broken (preserved) between the terminals. We have achieved these symmetry conditions by designing our MTJJs such that the graphene channel is symmetric between some but not all of the terminals. This design has allowed us to engineer reconfigurable nonreciprocal properties in our MTJJs. We have further studied the impact of a control bias current on the efficiency of nonreciprocal transport. We have also demonstrated nonreciprocity that is independent of the bias current polarity. This polarity-independent two-port nonreciprocity might potentially be useful for quantum applications where directional transport for drive and read-out microwave signals are required. Overall, our findings demonstrate the potential for exploiting MTJJs as a reconfigurable platform to engineer magnetic-field-free multiport devices for applications in low-temperature superconducting logics [50] and directional cryogenic devices [51].

The data supporting the conclusions of this letter is available on Zenodo [52].

ACKNOWLEDGMENTS

We acknowledge funding from the National Science Foundation (NSF) Innovation and Technology Ecosystems (Grant No. 2040667). F.Z. and N.S. acknowledge support from the University of Chicago. G.J.C. acknowledges support from the ARAP program of the Office of the Secretary of Defense. M.J.G. and M.T.A. acknowledge funding from US ARO Grant No. W911NF-20-2-0151 and the NSF through the University of Illinois at Urbana-Champaign Materials Research Science and Engineering Center DMR-1720633. K.W. and T.T. acknowledge support from the JSPS KAKENHI (Grants No. 19H05790, No. 20H00354, and No. 21H05233).

APPENDIX A: STOCHASTIC SWITCHING NOISE AT $T = 12$ mK

Figure 5 plots the histogram of the critical currents $I_{c,12}^{+}$ and $I_{c,21}^{+}$ at two different temperatures: $T = 12$ mK (a) and $T = 250$ mK (b) for the three-terminal JJ of the main text. We observe that at $T = 12$ mK, the device exhibits significant stochastic switching noise. However, the switching noise almost vanishes at $T = 250$ mK.

APPENDIX B: DIFFERENTIAL RESISTANCE MAPS FROM THE THREE-TERMINAL JJ IN CONFIG. 2.

Figure 6 plots the differential resistance dV_1/dI_1 and dV_2/dI_2 maps versus I_1 and I_2 for the three-terminal JJ of

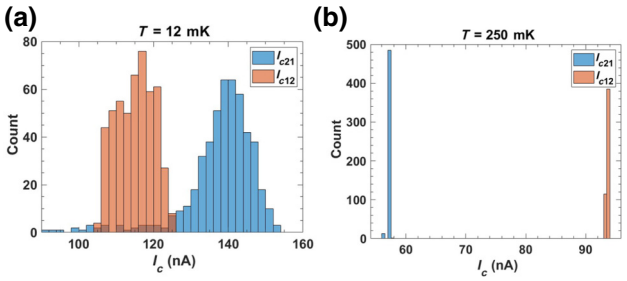

FIG. 5. (a),(b) Histogram of critical currents $I_{c,12}^{+}$ and $I_{c,21}^{+}$ in the three-terminal JJ of the main text, measured at $T = 12$ mK (a) and $T = 250$ mK (b).

the main text in config. 2. In (a) [(b)], we sweep I_1 (I_2) for each fixed I_2 (I_1) value. In this configuration, terminal 3 is grounded.

APPENDIX C: NONRECIPROCAL TRANSPORT IN A SECOND ASYMMETRIC THREE-TERMINAL JJ

Figure 7 plots the voltage-current characteristics of another asymmetric three-terminal JJ in config. 2. Here, we also observe nonreciprocal transport between terminals 1 and 2, which have no mirror symmetry. The efficiency is $\eta_{12}^{+} \approx 16\%$. The inset in each panel shows the bias configuration.

APPENDIX D: NONRECIPROCAL TRANSPORT IN THE FOUR-TERMINAL JJ

Figures 8(a) and 8(b) plot the critical currents $I_{c,12}^{\pm}$ and $I_{c,21}^{\pm}$ (a) and efficiency η_{12}^{+} as a function of the control current I_4 in the four-terminal JJ of the main text. The inset of Fig. 8(a) shows the bias configuration. At $I_4 = 0$, we observe that the critical current $I_{c,12}^{\pm} \neq I_{c,21}^{\pm}$, indicating that transport between these two terminals is nonreciprocal. Similar to the three-terminal case, this nonreciprocity is due to the asymmetric geometry of the graphene channel. We further observe that a nonzero I_4 creates an imbalance between positive and negative critical current polarities. We observe that while nonreciprocal transport is polarity independent for $I_4 = 0$, it becomes polarity dependent for $I_4 \neq 0$, i.e., $\eta_{12}^{+} \neq \eta_{21}^{+}$. However, we note that the average value of $\eta_{12}^{\text{avg}} = (\eta_{12}^{+} + \eta_{12}^{-})/2 \approx 20\%$ remains approximately constant. Therefore, we conclude that mirror symmetry breaking is responsible for nonreciprocal transport, whereas a control bias current simply creates a polarity-dependent imbalance between the critical currents.

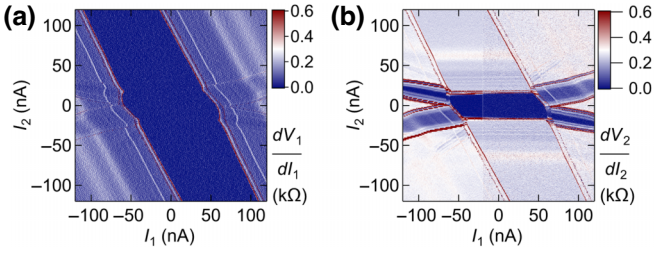

FIG. 6. Differential resistance maps measured in the three-terminal JJ of the main text in config. 2. (a),(b) Color map of the differential resistance dV_1/dI_1 (a) and dV_2/dI_2 (b) versus I_1 and I_2 in config 2.

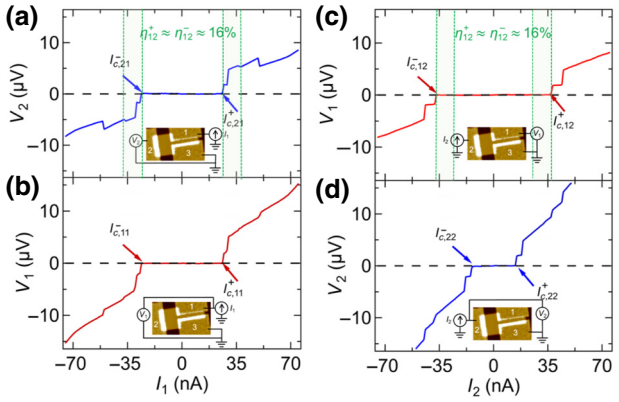

FIG. 7. (a),(b) Voltages V_2 (a) and V_1 (b) as a function of the bias current I_1 at $I_2 = 0$ nA. (c),(d) Voltages V_1 (c) and V_2 (d) as a function of the bias current I_2 at $I_1 = 0$ nA. The inset in each panel shows the measurement configuration. In each measurement, I_1 (or I_2) is swept from 0 to 100 nA in the positive direction and from 0 to −100 nA in the negative direction. The critical currents are labeled as $I_{c,11}^{\pm}$, $I_{c,21}^{\pm}$, $I_{c,12}^{\pm}$, and $I_{c,22}^{\pm}$. Shaded areas in (a) and (c) mark the range of the current in which transport is nonreciprocal. The efficiency of two-port nonreciprocity are calculated as $\eta_{12}^{+} \approx \eta_{12}^{-} \approx 16\%$.

APPENDIX E: SINGLE-PORT TREATMENT OF MTJJS AND ASYMMETRIC CRITICAL CURRENTS

In the three-terminal JJ of the main text, we observe that for nonzero I_2, the critical current at terminal 1 ($I_{c,11}$) is asymmetric for positive and negative current polarities [Fig. 1(d) of the main text]. This asymmetry may be interpreted as a signature of nonreciprocal transport in three-terminal JJs. However, this interpretation is based on a single-port definition of the critical current, and as

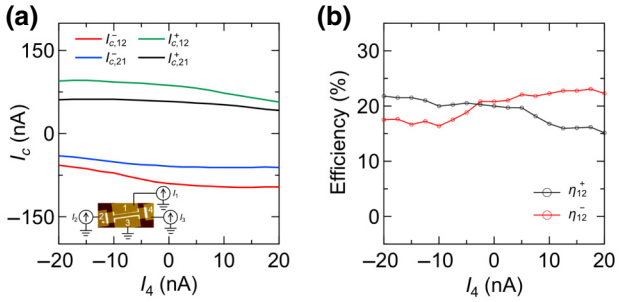

FIG. 8. Nonreciprocal transport in the four-terminal JJ of the main text, measured between terminals 1 and 2. (a) Critical currents versus the bias current I_4 extracted from V-I characteristics of a four-terminal JJ. Inset shows the measurement configuration. Here, terminal 3 is grounded and I_4 is kept at a constant value during each measurement. (b) Efficiency of nonreciprocal transport $\eta_{12}^{\pm}$ as a function of I_4.

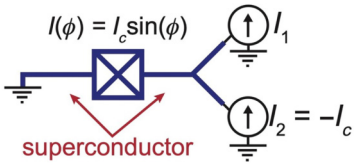

FIG. 9. Schematic of a two-terminal JJ connected to two current sources. The current in the JJ (I_{JJ}) is the sum of I_1 and I_2. If $I_2 = -I_c$, where I_c is the critical current of the JJ, $I_{JJ} = I_1 - I_c$. In this setup, the JJ is in the superconducting state for $0 \le I_1 \le 2I_c$, resulting in $I^+_{c,11} = 2I_c$ and $I^-_{c,11} = 0$. Therefore, if $I_{c,11}$ is solely used to characterize the JJ, one might assume the device is nonreciprocal, even though the JJ itself is reciprocal. This toy example highlights the limitations of using the single-port definition of nonreciprocity in multiport networks.

we argue in the following is not applicable in multiport devices. In the schematic of Fig. 9, we consider a reciprocal two-terminal JJ with a critical current I_c. We further assume that the left terminal is grounded but the right terminal is connected through superconducting leads to two current sources (I_1 and I_2). If $I_2 = -I_c$, $I_{JJ} = I_1 + I_2 = I_1 - I_c$. In this case, when $I_1 = 2I_c$, $I_{JJ} = I_1 - I_c = I_c$ and the JJ will transition to normal state. Following the single-port definition of nonreciprocity, this value of I_1 is considered $I^+_{c1} = 2I_c$. On the other hand, when $I_1 = 0$, $I_{JJ} = I_1 - I_c = -I_c$. This value is then considered I^-_{c1}. Consequently, in this three-terminal system, $I^+_{c1} \neq I^-_{c1}$. However, as we noted earlier the two-terminal JJ is reciprocal. We note that the use of superconducting leads ensures that the current injected into the JJ is dissipationless. Therefore, even though the underlying current-phase relation of the three-terminal JJ may be asymmetric with the sign reversal of the phase at $I_2 \neq 0$, $[I_1(\Phi_1, I_2) \neq -I_1(-\Phi_1, I_2)]$, it is experimentally challenging to distinguish reciprocal and nonreciprocal devices using the single-port definition of nonreciprocity.

APPENDIX F: THE RESISTIVELY SHUNTED JUNCTION MODEL PARAMETERS

We use the RSJ model similar to our previous work [41] to numerically simulate our three-terminal junctions. Here, we assume the capacitance of the junction is zero. Following Ref. [41], for our three-terminal device, we obtain

$$\mathbf{I} = \mathbf{f}(\tau) + \mathcal{G} \cdot \frac{d\Phi(\tau)}{d\tau}. \tag{F1}$$

where $\mathbf{I} = (I_1/I_c, I_2/I_c)^T$, $\Phi = (\phi_1(\tau), \phi_2(\tau))^T$, and

$$\mathbf{f}(\tau) = \begin{pmatrix} I_{c3}\sin\phi_{13} + I_{c1}\sin\phi_1 \\ I_{c2}\sin\phi_{23} + I_{c1}\sin\phi_2 \end{pmatrix}. \tag{F2}$$

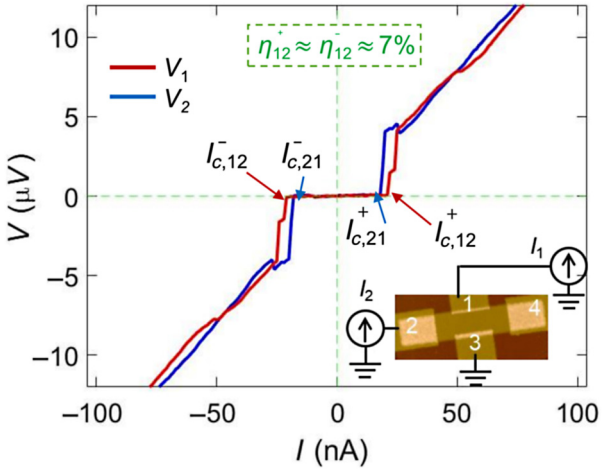

FIG. 10. Nonreciprocal transport in a second four-terminal JJ. Voltages V_1 and V_2 versus bias currents I_2 and I_1 at $I_1 = 0$ nA and $I_2 = 0$ nA, respectively. Arrows indicate the critical currents as $I^+_{c,12}, I^+_{c,21}, I^-_{c,12}$, and $I^-_{c,21}$. The efficiency of two-port nonreciprocity is $\eta^+_{12} \approx \eta^-_{12} \approx 7\%$.

In the above equations, $\tau = t/\tau_J$, where $t/\tau_J = \hbar/2eRI_c$ with $R = 1\ \Omega$ and $I_c = 10$ nA. The parameters of our RSJ model are: $G_{12} = G_{23} = 1/115\ (1/\Omega)$, $G_{13} = xG_{12}$, and $I_{c1} = I_{c2} = 1.3, I_{c3} = xI_{c1}$.

APPENDIX G: DEPENDENCE OF NONRECIPROCAL EFFICIENCY ON CHANNEL ASYMMETRY

Figure 10 plots the voltage-current characteristics of another four-terminal JJ, where the graphene channel is more symmetric compared to the four-terminal JJ presented in the main text. Here, we observe a nonreciprocal efficiency of $\eta^{\pm}_{12} \approx 7\%$, which is smaller compared to the four-terminal device of the main text. This observation

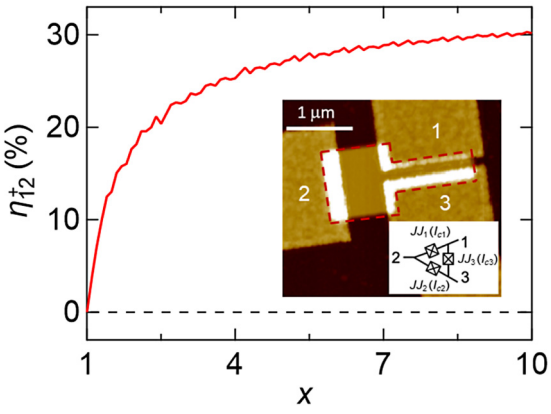

FIG. 11. Theoretical simulation of the efficiency η^+_{12} using the RSJ model. The value of x represents the degree of asymmetry in the three-terminal JJ as $x = I_{c3}/I_{c1} = I_{c3}/I_{c2}$.

highlights the relevance of mirror symmetry in determining the MTJJ's nonreciprocity. To better understand the dependence of η on the channel asymmetry, we perform numerical simulations based on resistively shunted junction model. Using the circuit-network model presented in the main text [inset of Fig. 1(b)], we characterize the broken spatial mirror symmetry as the ratio between the critical currents of JJ3 and JJ1/JJ2 (i.e., $x = I_{c3}/I_{c1} = I_{c3}/I_{c2}$). In this case, $x = 1$ represents the perfect mirror symmetry. Our modeling shows that the efficiency increases with increasing x and eventually plateaus at approximately 30% (Fig. 11). This maximum theoretical η is comparable to our observed nonreciprocal efficiency of $\eta \approx 24\%$ in the three-terminal JJ.

[1] L. Onsager, Reciprocal relations in irreversible processes. I., Phys. Rev. **37**, 405 (1931).

[2] J. Scaff and R. Ohl, Development of silicon crystal rectifiers for microwave radar receivers, Bell Syst. Tech. J. **26**, 1 (1947).

[3] W. Shockley, The theory of p-n junctions in semiconductors and p-n junction transistors, Bell Syst. Tech. J. **28**, 435 (1949).

[4] E. Monroy, F. Omnès, and F. Calle, Wide-bandgap semiconductor ultraviolet photodetectors, Semicond. Sci. Technol. **18**, R33 (2003).

[5] S. M. Sze, *Semiconductor Devices: Physics and Technology* (John Wiley & Sons, Inc., Hoboken, New Jersey, 2008).

[6] J. Hu, C. Wu, and X. Dai, Proposed design of a Josephson diode, Phys. Rev. Lett. **99**, 067004 (2007).

[7] R. Wakatsuki and N. Nagaosa, Nonreciprocal current in noncentrosymmetric Rashba superconductors, Phys. Rev. Lett. **121**, 026601 (2018).

[8] S. Hoshino, R. Wakatsuki, K. Hamamoto, and N. Nagaosa, Nonreciprocal charge transport in two-dimensional noncentrosymmetric superconductors, Phys. Rev. B **98**, 054510 (2018).

[9] C.-Z. Chen, J. J. He, M. N. Ali, G.-H. Lee, K. C. Fong, and K. T. Law, Asymmetric Josephson effect in inversion symmetry breaking topological materials, Phys. Rev. B **98**, 075430 (2018).

[10] M. Davydova, S. Prembabu, and L. Fu, Universal Josephson diode effect, Sci. Adv. **8**, eabo0309 (2022).

[11] A. Daido, Y. Ikeda, and Y. Yanase, Intrinsic superconducting diode effect, Phys. Rev. Lett. **128**, 037001 (2022).

[12] H. D. Scammell, J. Li, and M. S. Scheurer, Theory of zero-field superconducting diode effect in twisted trilayer graphene, 2D Mater. **9**, 025027 (2022).

[13] N. F. Yuan and L. Fu, Supercurrent diode effect and finite-momentum superconductors, Proc. Natl. Acad. Sci. **119**, e2119548119 (2022).

[14] S. Ilić and F. Bergeret, Theory of the supercurrent diode effect in Rashba superconductors with arbitrary disorder, Phys. Rev. Lett. **128**, 177001 (2022).

[15] J. J. He, Y. Tanaka, and N. Nagaosa, A phenomenological theory of superconductor diodes, New J. Phys. **24**, 053014 (2022).

[16] Y. Zhang, Y. Gu, P. Li, J. Hu, and K. Jiang, General theory of Josephson diodes, Phys. Rev. X **12**, 041013 (2022).

[17] F. Ando, Y. Miyasaka, T. Li, J. Ishizuka, T. Arakawa, Y. Shiota, T. Moriyama, Y. Yanase, and T. Ono, Observation of superconducting diode effect, Nature **584**, 373 (2020).

[18] J. Diez-Merida, A. Díez-Carlón, S. Yang, Y.-M. Xie, X.-J. Gao, K. Watanabe, T. Taniguchi, X. Lu, K. T. Law, and D. K. Efetov, Magnetic Josephson junctions and superconducting diodes in magic angle twisted bilayer graphene, ArXiv:2110.01067 (2021).

[19] J. Yun, S. Son, J. Shin, G. Park, K. Zhang, Y. J. Shin, J.-G. Park, and D. Kim, Magnetic proximity-induced superconducting diode effect and infinite magnetoresistance in a van der Waals heterostructure, Phys. Rev. Res. **5**, L022064 (2023).

[20] C. Baumgartner, L. Fuchs, A. Costa, S. Reinhardt, S. Gronin, G. C. Gardner, T. Lindemann, M. J. Manfra, P. E. Faria Junior, D. Kochan, *et al.*, Supercurrent rectification and magnetochiral effects in symmetric Josephson junctions, Nat. Nanotechnol. **17**, 39 (2022).

[21] H. Narita, J. Ishizuka, R. Kawarazaki, D. Kan, Y. Shiota, T. Moriyama, Y. Shimakawa, A. V. Ognev, A. S. Samardak, Y. Yanase, *et al.*, Field-free superconducting diode effect in noncentrosymmetric superconductor/ferromagnet multilayers, Nat. Nanotechnol. **17**, 823 (2022).

[22] K.-R. Jeon, J.-K. Kim, J. Yoon, J.-C. Jeon, H. Han, A. Cottet, T. Kontos, and S. S. Parkin, Zero-field polarity-reversible Josephson supercurrent diodes enabled by a proximity-magnetized pt barrier, Nat. Mater. **21**, 1008 (2022).

[23] L. Bauriedl, C. Bäuml, L. Fuchs, C. Baumgartner, N. Paulik, J. M. Bauer, K.-Q. Lin, J. M. Lupton, T. Taniguchi, K. Watanabe, *et al.*, Supercurrent diode effect and magnetochiral anisotropy in few-layer $NbSe_2$, Nat. Commun. **13**, 1 (2022).

[24] B. Pal, A. Chakraborty, P. K. Sivakumar, M. Davydova, A. K. Gopi, A. K. Pandeya, J. A. Krieger, Y. Zhang, S. Ju, N. Yuan, *et al.*, Josephson diode effect from cooper pair momentum in a topological semimetal, Nat. Phys. **18**, 1228 (2022).

[25] H. Wu, Y. Wang, Y. Xu, P. K. Sivakumar, C. Pasco, U. Filippozzi, S. S. Parkin, Y.-J. Zeng, T. McQueen, and M. N. Ali, The field-free Josephson diode in a van der Waals heterostructure, Nature **604**, 653 (2022).

[26] J.-X. Lin, P. Siriviboon, H. D. Scammell, S. Liu, D. Rhodes, K. Watanabe, T. Taniguchi, J. Hone, M. S. Scheurer, and J. Li, Zero-field superconducting diode effect in small-twist-angle trilayer graphene, Nat. Phys. **18**, 1221 (2022).

[27] S. Matsuo, T. Imoto, T. Yokoyama, Y. Sato, T. Lindemann, S. Gronin, G. C. Gardner, M. J. Manfra, and S. Tarucha, Josephson diode effect derived from short-range coherent coupling, Nat. Phys. **19**, 1641 (2023).

[28] M. Gupta, G. V. Graziano, M. Pendharkar, J. T. Dong, C. P. Dempsey, C. Palmstrøm, and V. S. Pribiag, Gate-tunable superconducting diode effect in a three-terminal Josephson device, Nat. Commun. **14**, 3078 (2023).

[29] J. Chiles, E. G. Arnault, C.-C. Chen, T. F. Q. Larson, L. Zhao, K. Watanabe, T. Taniguchi, F. Amet, and G.

Finkelstein, Nonreciprocal supercurrents in a field-free graphene Josephson triode, Nano. Lett. **23**, 5257 (2023).
[30] M. Alidoust, G. Sewell, and J. Linder, Superconducting phase transistor in diffusive four-terminal ferromagnetic Josephson junctions, Phys. Rev. B **85**, 144520 (2012).
[31] A. H. Pfeffer, J. E. Duvauchelle, H. Courtois, R. Mélin, D. Feinberg, and F. Lefloch, Subgap structure in the conductance of a three-terminal Josephson junction, Phys. Rev. B **90**, 075401 (2014).
[32] Y. Cohen, Y. Ronen, J.-H. Kang, M. Heiblum, D. Feinberg, R. Mélin, and H. Shtrikman, Nonlocal supercurrent of quartets in a three-terminal Josephson junction, Proc. Natl. Acad. Sci. **115**, 6991 (2018).
[33] A. W. Draelos, M.-T. Wei, A. Seredinski, H. Li, Y. Mehta, K. Watanabe, T. Taniguchi, I. V. Borzenets, F. Amet, and G. Finkelstein, Supercurrent flow in multiterminal graphene Josephson junctions, Nano Lett. **19**, 1039 (2019).
[34] N. Pankratova, H. Lee, R. Kuzmin, K. Wickramasinghe, W. Mayer, J. Yuan, M. G. Vavilov, J. Shabani, and V. E. Manucharyan, Multiterminal Josephson effect, Phys. Rev. X **10**, 031051 (2020).
[35] G. V. Graziano, J. S. Lee, M. Pendharkar, C. J. Palmstrøm, and V. S. Pribiag, Transport studies in a gate-tunable three-terminal Josephson junction, Phys. Rev. B **101**, 054510 (2020).
[36] E. G. Arnault, S. Idris, A. McConnell, L. Zhao, T. F. Larson, K. Watanabe, T. Taniguchi, G. Finkelstein, and F. Amet, Dynamical stabilization of multiplet supercurrents in multiterminal Josephson junctions, Nano Lett. **22**, 7073 (2022).
[37] K.-F. Huang, Y. Ronen, R. Mélin, D. Feinberg, K. Watanabe, T. Taniguchi, and P. Kim, Evidence for 4e charge of cooper quartets in a biased multi-terminal graphene-based Josephson junction, Nat. Commun. **13**, 3032 (2022).
[38] G. V. Graziano, M. Gupta, M. Pendharkar, J. T. Dong, C. P. Dempsey, C. Palmstrøm, and V. S. Pribiag, Selective control of conductance modes in multi-terminal Josephson junctions, Nat. Commun. **13**, 1 (2022).
[39] R. Mélin and D. Feinberg, Quantum interferometer for quartets in superconducting three-terminal Josephson junctions, Phys. Rev. B **107**, L161405 (2023).
[40] R. Mélin, R. Danneau, and C. B. Winkelmann, Proposal for detecting the π-shifted cooper quartet supercurrent, Phys. Rev. Res. **5**, 033124 (2023).
[41] F. Zhang, A. S. Rashid, M. T. Ahari, W. Zhang, K. M. Ananthanarayanan, R. Xiao, G. J. de Coster, M. J. Gilbert, N. Samarth, and M. Kayyalha, Andreev processes in mesoscopic multiterminal graphene Josephson junctions, Phys. Rev. B **107**, L140503 (2023).
[42] R.-P. Riwar, M. Houzet, J. S. Meyer, and Y. V. Nazarov, Multi-terminal Josephson junctions as topological matter, Nat. Commun. **7**, 11167 (2016).
[43] E. Strambini, S. D'Ambrosio, F. Vischi, F. Bergeret, Y. V. Nazarov, and F. Giazotto, The ω-squipt as a tool to phase-engineer Josephson topological materials, Nat. Nanotechnol. **11**, 1055 (2016).
[44] J. S. Meyer and M. Houzet, Nontrivial Chern numbers in three-terminal Josephson junctions, Phys. Rev. Lett. **119**, 136807 (2017).
[45] H. B. G. Casimir, On Onsager's principle of microscopic reversibility, Rev. Mod. Phys. **17**, 343 (1945).
[46] L. J. van der Pauw, A method of measuring specific resistivity and Hall effect of discs of arbitrary shape, Philips Res. Rep. **13**, 1 (1958). https://aki.issp.u-tokyo.ac.jp/okano/WalWiki/etc/VDP_PRR_13_1.pdf
[47] M. Büttiker, Four-terminal phase-coherent conductance, Phys. Rev. Lett. **57**, 1761 (1986).
[48] T. Fulton and L. Dunkleberger, Lifetime of the zero-voltage state in Josephson tunnel junctions, Phys. Rev. B **9**, 4760 (1974).
[49] J. Clarke, A. N. Cleland, M. H. Devoret, D. Esteve, and J. M. Martinis, Quantum mechanics of a macroscopic variable: The phase difference of a Josephson junction, Science **239**, 992 (1988).
[50] T. Golod and V. M. Krasnov, Demonstration of a superconducting diode-with-memory, operational at zero magnetic field with switchable nonreciprocity, Nat. Commun. **13**, 1 (2022).
[51] C. Leroux, A. Parra-Rodriguez, R. Shillito, A. Di Paolo, W. D. Oliver, C. M. Marcus, M. Kjaergaard, A. Gyenis, and A. Blais, Nonreciprocal devices based on voltage-tunable junctions, ArXiv:2209.06194 (2022).
[52] https://doi.org/10.5281/zenodo.8066318.